
AFRL-RX-WP-TP-2012-0386

# ADAPTION OF AN IN-SITU MICROSCALE TENSION TECHNIQUE TO ENABLE FATIGUE TESTING (PREPRINT)

**J.M. Larsen, C.J. Szczepanski, and P.A. Shade**
**Metals Branch**
**Structural Materials Division**

**R. Wheeler**
**UES, Inc.**

**S.K. Jha**
**Wright State University**

**AUGUST 2012**
**Interim**



**AIR FORCE RESEARCH LABORATORY**
**MATERIALS AND MANUFACTURING DIRECTORATE**
**WRIGHT-PATTERSON AIR FORCE BASE, OH 45433-7750**
**AIR FORCE MATERIEL COMMAND**
**UNITED STATES AIR FORCE**

# REPORT DOCUMENTATION PAGE

*Form Approved*
*OMB No. 0704-0188*



| 1. REPORT DATE *(DD-MM-YY)* | 2. REPORT TYPE | 3. DATES COVERED *(From - To)* |
|---|---|---|
| August 2012 | Technical Paper | 1 July 2012 – 1 August 2012 |

**4. TITLE AND SUBTITLE**
ADAPTION OF AN IN-SITU MICROSCALE TENSION TECHNIQUE TO ENABLE FATIGUE TESTING (PREPRINT)

**5a. CONTRACT NUMBER**
In-house

**5b. GRANT NUMBER**

**5c. PROGRAM ELEMENT NUMBER**
62102F

**6. AUTHOR(S)**
J.M. Larsen, C.J. Szczepanski, and P.A. Shade (AFR./RXCM)
R. Wheeler (UES, Inc.)
S.K. Jha (Wright State University)

**5d. PROJECT NUMBER**
4347

**5e. TASK NUMBER**
20

**5f. WORK UNIT NUMBER**
X071

**7. PERFORMING ORGANIZATION NAME(S) AND ADDRESS(ES)**
Metals Branch (AFRL/RXCM)
Structural Materials Division
Air Force Research Laboratory, Materials and Manufacturing Directorate
Wright-Patterson Air Force Base, OH 45433-7750
Air Force Materiel Command, United States Air Force

**8. PERFORMING ORGANIZATION REPORT NUMBER**
AFRL-RX-WP-TP-2012-0386

**9. SPONSORING/MONITORING AGENCY NAME(S) AND ADDRESS(ES)**
Air Force Research Laboratory
Materials and Manufacturing Directorate
Wright-Patterson Air Force Base, OH 45433-7750
Air Force Materiel Command
United States Air Force

**10. SPONSORING/MONITORING AGENCY ACRONYM(S)**
AFRL/RXCM

**11. SPONSORING/MONITORING AGENCY REPORT NUMBER(S)**
AFRL-RX-WP-TP-2012-0386

**12. DISTRIBUTION/AVAILABILITY STATEMENT**
Approved for public release; distribution unlimited. Preprint to be submitted to International Journal of Fatigue.

**13. SUPPLEMENTARY NOTES**
The U.S. Government is joint author of this work and has the right to use, modify, reproduce, release, perform, display, or disclose the work. PA Case Number and clearance date: 88ABW-2012-3016, 23 May 2012. This document contains color.

**14. ABSTRACT**
Under high cycle and very high cycle fatigue (HCF and VHCF) conditions, scatter in fatigue lifetimes is substantial; often 2-3 orders of magnitude. Characterization of fatigue crack initiation sites in laboratory scale fatigue specimens has led to the identification of characteristic initiation sites and microstructural arrangements. Despite these observations, in some cases, it is still unclear how apparently similar initiation sites exhibit such different total fatigue lifetimes. Differences in crack-initiation mechanisms can be further revealed if specific microstructural arrangements are isolated to a micro-specimen. Towards this end, an in-situ microscale tension testing technique was adapted to enable microscale fatigue testing on tensile dog-bone specimens. Microscale tensile fatigue specimens with approximate gage diameters of 20 micrometers were prepared with a focused ion beam (FIB) microscope. Initial tensile experiments were conducted to characterize the mechanical behavior of microscale specimens for this microstructure. The microscale tensile specimens were observed to exhibit poorer mechanical properties than bulk tensile specimens.

**15. SUBJECT TERMS**
Titanium Alloys, Fatigue Test, Electron Backscatter Diffraction (EBSD), microscale mechanical testing

| 16. SECURITY CLASSIFICATION OF: | | | 17. LIMITATION OF ABSTRACT: | NUMBER OF PAGES | 19a. NAME OF RESPONSIBLE PERSON (Monitor) |
|---|---|---|---|---|---|
| a. REPORT | b. ABSTRACT | c. THIS PAGE | | | Andrew Rosenberger |
| Unclassified | Unclassified | Unclassified | SAR | 32 | 19b. TELEPHONE NUMBER *(Include Area Code)* N/A |

# Adaptation of an *in-situ* Microscale Tension Technique to Enable Fatigue Testing

C.J. Szczepanski, S.K. Jha[1], P.A. Shade, R. Wheeler[2], J.M. Larsen
US Air Force Research Laboratory, AFRL/RX, Wright-Patterson AFB, OH 45433
[1]Universal Technology Corporation, Dayton, OH 45432
[2] UES, Inc., Dayton, OH

## Abstract

*Keywords* (max 5 words)
Titanium Alloys, Fatigue Test, Electron Backscatter Diffraction (EBSD), microscale mechanical testing

Under high cycle and very high cycle fatigue (HCF and VHCF) conditions, scatter in fatigue lifetimes is substantial; often 2-3 orders of magnitude. Characterization of fatigue crack initiation sites in laboratory scale fatigue specimens has led to the identification of characteristic initiation sites and microstructural arrangements. Despite these observations, in some cases, it is still unclear how apparently similar initiation sites exhibit such different total fatigue lifetimes. Differences in crack-initiation mechanisms can be further revealed if specific microstructural arrangements are isolated to a micro-specimen. Towards this end, an *in-situ* microscale tension testing technique was adapted to enable microscale fatigue testing on tensile dog-bone specimens. Microscale tensile fatigue specimens with approximate gage diameters of 20 micrometers were prepared with a focused ion beam (FIB) microscope. Initial tensile experiments were conducted to characterize the mechanical behavior of microscale specimens for this microstructure. The microscale tensile specimens were observed to exhibit poorer mechanical properties than bulk tensile specimens. However, in this feasibility demonstration of *in-situ* microscale fatigue testing, microscale specimens exhibit enhanced fatigue properties relative to conventional specimens. Both tensile and fatigue specimens have been characterized with orientation imaging microscopy to identify the neighborhood and the specific slip systems that were activated under local deformation conditions within the microstructure. Both basal and prism slip were observed, although prism slip was more prevalent. Results of both the tension and fatigue tests are discussed in the context of the growing body of literature on microscale testing, and avenues for future work are highlighted.

## Introduction

In the high cycle and very high cycle fatigue (HCF and VHCF) regimes, the variability in fatigue behavior may constitute 2-3 orders of magnitude.[1,2] This scatter in lifetimes is attributed to the role of microstructural heterogeneity, leading to variability in fatigue crack initiation processes. At stresses up to approximately 80% of the bulk yield stress, the bulk plastic strain accumulation is considered to be negligible, and only localized plasticity is observed to accumulate in fatigue-critical microstructural locations. Previous research on the fatigue behavior of Ti-6Al-2Sn-4Zr-6Mo (subsequently referred to as Ti-6246), and subsequent characterization of specimens via sectioning and electron microscopy, have enabled the identification of specific microstructural neighborhoods that are likely to initiate fatigue cracks.[2-4] It is believed that this hierarchy of fatigue-critical microstructural neighborhoods drives fatigue lifetime variability. Despite the post-mortem identification and detailed characterization of these neighborhoods, the microstructural neighborhood surrounding fatigue crack initiation sites for specimens with long and short fatigue lifetimes are often indistinguishable. In addition, the fatigue-critical microstructural neighborhoods are not anomalous relative to the nominal material. Thus, it is believed that the mechanism of fatigue damage accumulation at these sites may drive the variable fatigue behavior observed in these specimens. An *in-situ* microscale fatigue testing technique has been employed to enable a fundamental understanding of the fatigue damage accumulation processes preceding fatigue crack initiation.

Due to the anisotropic mechanical behavior of the hexagonal close packed (HCP) α phase in titanium and the absence of inclusions and porosity, the mechanical properties, including fatigue performance, are strongly related to the crystallographic texture of these alloys.[5-7] With the combined use of focused ion beam (FIB) and electron backscattered diffraction (EBSD) techniques, researchers have been able to characterize microstructural neighborhoods that promote fatigue crack initiation.[3,8,9] Fatigue crack initiation sites in duplex Ti alloys are often primary α ($\alpha_p$) grains that are favorably oriented for either basal or prism slip,[2,10] which are the two slip systems with the lowest critical resolved shear stress (CRSS).[11] Previous research on this alloy has found that the fatigue crack initiation sites are not simply anomalously large $\alpha_p$ grains, nor are the surrounding microstructural neighborhoods especially unique relative to the bulk material.[2]

Fatigue crack initiation in duplex titanium alloys has been studied by many researchers, and this has yielded numerous proposed mechanisms of cyclic damage accumulation leading to fatigue crack initiation.[12-16] The interaction of slip between hard and soft oriented grains has led researchers to propose the so-called Stroh mechanism, where it is believed that cracks form in grains with a hard orientation (c-axis || loading axis) due to slip occurring in an adjacent soft-oriented grain, which ultimately leads to crack formation.[14,15] Although recent work has contradicted the specific details of this mechanism,[16] it is clear that the interaction of slip activity between adjacent hard and soft grains is an important process controlling mechanical behavior. A mechanism of crack initiation attributed to strain incompatibility at phase boundaries has been cited by other researchers, as well.[13] In their work, Mahajan and Margolin identify crack initiation at phase interfaces in low strain testing, while at higher applied loads, they report formation of continuous slip bands across α grain boundaries. Others have observed that fatigue damage accumulates easily across multiple grains sharing similar crystallographic orientations.[9,16,17] Furthermore, accurate descriptions of the crack initiation mechanisms must consider the orientations of both the α and β phases, since their relative crystallographic orientations will strongly affect the ability of slip to be transmitted across phase boundaries under monotonic loading conditions.[18-20] However, it is not clear if the loading about certain orientations satisfying the Burgers orientation relationship would allow for easier slip transmission across the α/β interface under cyclic loading conditions in titanium alloys. The approach of *in-situ* microscale testing with combined EBSD analysis will aid in the identification of the active cyclic deformation mechanisms. Microscale specimens provide the advantage that a large volume fraction of the grains within the gage volume can be directly observed by monitoring the specimen surface. Additionally, these specimens are well suited for detailed characterization and analysis techniques, such as 3D serial sectioning, due to their relatively small volume.

Many researchers have investigated the monotonic mechanical response of microscale specimens and numerous reviews have been written on this subject.[21-24] Mechanical testing at this scale allows characterization of mechanical size effects, exploration of deformation micromechanisms, and measurement of the local properties in a bulk material (e.g., variations in the local response due to microstructural and chemical gradients in a bulk material).[25-27] Within the spectrum of

specimen sizes ranging from single crystals, to specimens containing only a few grains, and ultimately polycrystalline samples, various categories of behavior are observed. For specimen sizes on the order of a single grain and below, numerous researchers have demonstrated that yield strengths and flow stresses are typically higher than in bulk specimens, and the measured values continue to increase as the specimen size is reduced.[22,25,27-28] The work of Shade and coworkers has found that the yield strength of nickel-base superalloy microspecimens is typically higher than the yield strength of bulk crystals of the same material, even for microscale single crystal specimens as large as 80 μm in diameter.[27] Similarly, Norfleet illustrated that the yield strength and flow stress of single phase Ti-6Al and single colony Ti-6242 samples were also higher in microscale specimens than in bulk samples. However, it was noted that titanium alloys exhibited less sensitivity to specimen size than did FCC materials such as nickel and gold.[28] The absence of dislocation multiplication mechanisms in samples of this size is typically cited as the hardening mechanism in single crystal microscale tests. For specimens containing a few grains through the sample thickness, reports typically cite decreasing yield strength or flow stress as a function of decreasing specimen size and this has been variously attributed to the lack of constraint in surface connected grains compared with internal grains.[29-32] With even a few grain boundaries or phase interfaces, it is believed that there are sufficient dislocation sources and therefore the fraction of surface-connected grains dominates the mechanical behavior of these specimens. In copper microwires, Yang observed decreased flow stress as specimen size was reduced, which was attributed to this lack of grain constraint.[29] Janssen and coworkers independently varied specimen size and the microstructural scale and found that once the specimen thickness was reduced to the order of a few grain diameters, the measured yield and flow properties of these specimens were also diminished.[30] They attributed this result to the lack of constraint on grains at the specimen surface, which resulted in the facile propagation of plasticity, once it had localized. Khatibi et al. observed a reduction in cyclic mechanical properties in micro wires and attributed this to the ease of continued damage accumulation once it had localized in the form of a slip band on the specimen surface.[32] However, they were not able to decouple the effects of microstructural scale from the specimen size effects in their tests, due to the bamboo type microstructures present in microwires.

There are numerous reports in the literature regarding microscale fatigue testing. However, these efforts are typically targeted at characterizing the mechanical response of small scale structures such as thin films,[33] micro-wires,[29,34] solder interconnects,[35] or micro-electro-mechanical systems (MEMS).[36-38] Since small scale devices are intended for use in specific applications, much of the research on these devices often focuses on identifying the environmentally driven failure modes that occur during normal operation. The objective of the current work is to determine the fundamental role of cyclic damage accumulation mechanisms on fatigue crack initiation. Of particular interest are slip transmission and fatigue damage accumulation mechanisms that are active among the various constituent phases in this alloy. Proper identification of the active deformation mechanisms is intended to elucidate the fatigue-critical microstructural features at fatigue crack initiation sites in bulk fatigue specimens. Additionally, the results are intended to support the mechanism and parameter characterization needed for constitutive equations in crystal plasticity finite element analysis.

## Experimental Procedure

### *Material*

Material for this study came from the grip section of tested laboratory scale fatigue samples of Ti-6246; Figure 1 presents a backscattered electron (BSE) micrograph of the material. As reported elsewhere, the average grain size of the $\alpha_p$ grains is 3.7 μm ± 2.6 μm, but as this micrograph illustrates, grains with diameters as large as 10 μm are commonly observed throughout the microstructure.[2] The volume fraction of $\alpha_p$ is 27% ± 3% in this microstructure. This microstructural condition is composed of α laths (dark high-aspect ratio phase), which maintain the Burgers orientation relationship with the retained β phase material (bright matrix phase). The transformed β grains, which are composed of the α laths and the retained β phase, are typically on the order of 20 μm in diameter. Crack initiation sites were typically associated with microtextured regions, which were favorably oriented for easy basal and prism slip.[2] However, as the inverse pole figure (IPF) maps in Figure 2 illustrate, clusters of material that are favorably oriented for easy slip are commonly observed, even in nominal sections of material.

### *Specimen Preparation*

The source material for these microscale tests was a metallographic specimen was prepared via conventional metallographic techniques and finished with vibratory polishing on 0.05 μm colloidal silica, which yields a surface with low residual stress. Specimens for this work were fabricated through a combination of micro-electrodischarge machining (micro-EDM) and FIB milling.[39] A Sarix SX-100 micro-EDM was employed to machine cylindrical specimen blanks in the substrate measuring approximately 80 μm in diameter and approximately 100 μm in height. These blanks were subsequently FIB milled to produce a tensile sample geometry using an FEI Nova Nanolab FIB and a custom script for automated lathe milling.[39] Figure 3 is a micrograph of a batch of specimens in various stages of completion. The two pillars on the left of the image were produced via micro-EDM, while the three posts on the right were all subsequently machined via FIB. The FIB was operated at 30 kV and 9.3nA to obtain the rough specimen geometry. As the dimensions approached the desired specimen size, the probe current was reduced to 2.8 nA, and then ultimately to 0.92 nA, in order to increase milling precision and minimize the amount of material redeposited onto the specimen surfaces. Once the desired diameter was achieved, flats were machined on the front and back faces of the specimens to aid in acquiring EBSD patterns directly from the sample surface. Following this machining process, specimens were "cleaned" with a low energy ion beam (5kV, 1.5 nA) for a short duration to reduce ion damage from the initial 30 kV milling procedure. The low energy ion cleaning step significantly improved the quality of EBSD patterns that were acquired and improved contrast of the microstructural features in BSE images. As shown in Figure 4, specimen gage sections were typically 50 μm long and approximately 20 μm in diameter, while the grip head was nominally 40 μm in diameter. EBSD scans of the specimen surface were completed before testing each specimen to map the orientations of each grain on the observable portion of the specimen.

***Mechanical Testing***

Mechanical tests were completed *in-situ* in an FEI Quanta 6000 ESEM using a mechanical testing rig that was designed in-house, as shown in Figure 5.[26,40,41] This device has a three axis piezoelectric positioning stage used to manipulate and load the specimen within the grip. The grip is fabricated from silicon via microelectronic processing methods, and is intentionally designed to have very low lateral stiffness. Once the specimen is loaded in the grip, a piezoelectric actuator is used to apply a tensile load on the specimen. The grip is in series with a

1 kg. load cell. This micromechanical testing rig is controlled via custom Labview control software to apply the necessary voltage to the piezoelectric actuator to achieve the desired load levels. Images are taken periodically during the test to document displacement and to measure the onset of localized slip activity. The experiments are conducted in a quasi-static manner, where the actuator is held at a constant voltage value during image acquisition.

Strain was measured from the flat section of the specimen surface from secondary electron (SE) micrographs. Images were acquired using a 4Pi image acquisition system to capture images with a resolution of 6000 x 2000 pixels (~15 nm/pixel), which typically took about 3 minutes to acquire. This resolution allows for fine strains to be measured from micrographs. A one-pixel shift of a feature in these images typically corresponds to a total axial strain of $2.4 \times 10^{-4}$, considering that the gage length of the specimen is on the order of 4000 pixels. A MatLab script was used to align the images at the base of the specimen, and a correlation function was employed to measure the displacement of the fiducial marks during the test.

The microscale mechanical testing rig was adapted for the *in-situ* tensile fatigue tests. These tests are conducted via periodic calibration of the load to specified actuator displacements. The voltage applied to the actuator is thus calibrated to net section stress in the specimen. The minimum and maximum voltages to be applied to the actuator are determined from a quasi-static calibration procedure; these voltages correspond to the maximum and minimum stresses, respectively. Once the voltage range and mean voltage has been determined, a signal generator is activated to produce a sinusoidal waveform to activate the piezoelectric actuator at a frequencies varying from 1 Hz up to 100 Hz, with a stress ratio of R=0.05 at room temperature. The load trace for a one-hour block of a fatigue test is shown in Figure 6a. In this figure, one can see the blocks of fatigue cycles spanning the full range of load, followed by a hold at the mean load. Generally, blocks of 900 cycles were applied, and then the specimen was loaded to the mean load, and an image was acquired. Following image acquisition, the quasi-static calibration procedure was repeated to reset the maximum and minimum displacements and verify that the same load was being induced in the microspecimen. From the load trace in Figure 6b, one can see the cyclic load is being applied at a frequency of 1 Hz and that the minimum and maximum loads being applied to the specimen are constant.

## Results

Initially, tension tests were completed to characterize the typical variation in mechanical properties for specimens of this size. Subsequently, specimens were tested in fatigue according to the procedure outlined above. The results from monotonic and cyclic microscale tests will be discussed separately.

### *Tension Tests*

*Stress-Strain Behavior*

The tensile data acquired in these tests are shown in Figure 7. The 0.2% offset yield strength was measured to range from 800 MPa up to 990 MPa, which is below the bulk yield strength of 1140 MPa. Compared with conventional lab-scale specimens, which exhibit very little scatter in monotonic mechanical properties, there is substantial scatter in the mechanical properties of microscale specimens. This scatter in mechanical properties is expected, based on results in the literature for specimens of this size.[23] Due to the exacerbated effect that a few individual grains may have on the mechanical response of specimens of this size, one would expect wide scatter in the yield behavior. For comparison, Larson and Zarkades[7] reported variations in yield strength up to approximately 200 MPa (~20% of baseline $\sigma_{YS}$) as a function of orientation relative to the rolling direction in strongly textured plates. Under this context, the variation in yield behavior observed in microspecimens is not surprising, given that an individual 10 μm diameter $\alpha_p$ grain may occupy as much as 40% of the cross-sectional area. Additionally, the mechanical response of these specimens is complicated due to the presence of multiple phases, with the α laths obeying the Burgers orientation relationship while the $\alpha_p$ grains do not. Furthermore, the crystallographic orientations of the matrix β phase also will influence the mechanical response, although to a lesser degree than the α phase. Thus, the variation in mechanical properties as a function of crystallographic orientation could be expected to account for the scatter in yield strength.

The observation of consistently lower yield strengths in these microsamples compared to bulk specimens and single crystal microspecimens appears to substantiate the results of Janssen.[30] As described in the Introduction, microspecimens of this size, coupled with the fine scale

microstructure of this material, would be expected to exhibit a reduction in mechanical properties. For specimens of this size, it is clear that the majority of grains contained within the specimen gage volume are connected to the surface. Thus, these grains would be expected to deform more readily due to the free surface. Additionally, this fine scale duplex microstructure provides many potential locations for damage to accumulate. The combined effects of lack of grain constraint and the multiple sources of dislocation nucleation sites would be expected to produce reduced mechanical properties relative to bulk specimens.

*Deformation Mechanisms*

Figure 8a depicts a microscale tension specimen with an overlay of the inverse pole figure (IPF) maps of the specimen surface. Based on the measured crystallographic orientations, the plane traces can be plotted on these figures, and these are shown in Figure 8b for basal (purple) and prism (green) planes, which are known to be the easy slip systems in α + β titanium alloys. Figure 8c is a micrograph of the tensile specimen immediately preceding final failure. The specimen ultimately failed from slip bands within the $\alpha_p$ grain, which were continuous across the phase interface into the adjacent lath α. In this specimen, slip initiated within the $\alpha_p$ grain at the interface boundary and then propagated across the α grain and back into the transformed β region. As shown in the IPF map in Figure 8a, the grain of interest had nearly the same orientation as the adjacent lath α material. Additionally, this can be confirmed by the nearly parallel alignment of prism planes in Figure 8b. Thus, it is believed that this grain combination was more susceptible to damage accumulation since these prism slip planes were aligned across the phase boundary. A mechanism of slip transfer would be expected to be operative in these locations since it appears that the $\alpha_p$ grain and the adjacent α laths exhibited very similar orientations.

Figure 9 shows a similar set of micrographs for a specimen in which slip accumulation is essentially limited to the lath α constituent. As shown in Figure 9c, there are multiple sites of localized slip activity in this specimen, but none of those locations exhibit slip transmission across a phase interface. In fact, the phase interface appears to be a site of slip intensification with deepening slip steps. Again, the critical slip activity in this specimen appears to be due to

the activation of prism slip within these microstructural features. This specimen, labeled B02 in the stress-train curve in Figure 7, exhibits significantly more plasticity before failure than specimen B01, which is shown in Figure 8. This increased elongation to failure measured in specimen B02 appears to correlate with the observation of slip accumulation within multiple microstructural features.

Comparison of Figures 8 (c) and 9(c) with 8(b) and 9(b) respectively indicates that the locations where slip lines are observed in these specimens is attributable to the activation of prism slip. This is consistent with reports in the literature that cite prism slip as the active deformation mode in monotonic loading of $\alpha + \beta$ titanium alloys.[11,42] This perceived preference for prism slip appears to be more significant when one considers the crystallographic orientation of other grains within this specimen. Figure 10 displays the Schmid factor maps for prism (Figure 10a) and basal (Figure 10b) slip for the specimen shown in Figure 9 (Specimen B02) based on the macroscopically applied load, which does not take into account the local variations in stress state at the grain level. As depicted in the legend, the colors for these Schmid factor maps do not represent equivalent ranges; rather they are skewed to accentuate the differences for the very highest values in Schmid factor. As one can observe from the Schmid factor map for basal slip in Figure 10b, there are two adjacent grains that are very favorably oriented for easy basal slip. Furthermore, one of the grains adjacent to this pair has a very low Schmid factor, which may makes it a candidate for slip incompatibility at this interface. Despite these seemingly severe grain orientation combinations in this region of the specimen, only a few faint basal slip traces are observable, as shown in the micrograph in Figure 9c. Thus, these results appear to substantiate reports in the literature of the preference for prism slip over basal slip in specimens loaded under monotonic conditions.[42]

### ***Fatigue Tests***

*Mechanical Response*

Initial microscale fatigue tests have been completed as part of this study, and all fatigue specimens tested exhibited superior fatigue behavior relative to conventional bulk specimens. This is shown in the S-N curve in Figure 11, where data for two microscale fatigue tests are included on a plot of previously reported conventional fatigue data.[2] For the two successful

microscale fatigue tests, specimen failure was not observed despite increasing the applied stress. In one case, the microscale specimen was step tested at stresses where a broad range of lifetimes are observed, while the other specimen was tested at stresses approaching the yield strength measured in bulk specimens.

Figure 12a displays a micrograph of a microscale specimen that has been subjected to fatigue loading at increasing maximum applied stresses ranging from 860 up to 980 MPa, which are represented by the red squares in Figure 11. Figures 12b-d demonstrate the continuous intensification of slip lines within specific grains in the microscale fatigue specimen as the maximum stress is increased for the loading frequency of 100 Hz. The slip lines are predominantly located within the central $\alpha_p$ grain, as shown in Figure 12b, which is an image of the specimen after loading at 860 MPa for $10^7$ cycles. From the micrograph in Figure 12c, which was acquired after fatiguing the specimen a further $10^7$ cycles at 920MPa, the continued intensification of slip lines within the $\alpha_p$ grain is apparent, as is the onset of an additional slip line along the interface of an adjacent $\alpha$ lath. Figure 13d shows the micrograph for this region after a further $10^7$ cycles at a maximum stress of 980 MPa. The slip lines in the $\alpha_p$ grain and the adjacent $\alpha$ lath continue to intensify under these conditions, however these slip lines do not initiate a fatigue crack or lead to specimen failure.

Subsequent fatigue testing was completed at applied stresses higher than those investigated in bulk specimens (i.e. $\sigma_{max} \geq 1100$ MPa) and at 1 Hz, as indicated by the green triangles in Figure 11. Despite these differences in maximum applied stress and cyclic frequency, very similar slip activity and intensification was observed. Figure 13 displays micrographs of a specimen that was initially subjected to a maximum stress of 1100 MPa for 43,000 cycles, followed by 1140 MPa for 57,000 cycles. After 43,000 cycles at 1100 MPa, slip lines are observed to form in adjacent $\alpha_p$ grains (Figure 13c). The slip lines further intensified when the maximum applied stress was increased to 1140 MPa, which is the yield strength measured in bulk specimens (Figure 13d). However, although 57,000 cycles were applied at this stress, this did not lead to fatigue crack initiation or specimen failure as shown in Figure 13d. This result is interesting when one compares the fatigue behavior of microscale specimens to that observed in bulk

specimens where the longest lifetime observed at a stress of 1040 MPa was only 24,679 cycles.[1]

Despite the fact that fatigue crack initiation was not observed after approximately 100,000 cycles, the accumulation of plastic strain within the specimen appears to increase throughout the test as shown in the plot of strain accumulation in Figure 14. The annotations (i.e. A, B, C, and D) at the top of Figure 14 depict the point in time at which the corresponding images in Figure 13(a-d) were acquired. Further validation of these measurements is found in the observation of an increase in strain accumulation corresponding to an increase in the maximum applied stress immediately after point C in Figure 14.

Based on the EBSD data from the surface of this specimen, the grains that exhibit slip activity are favorably oriented for one of the two easy slip modes in $\alpha + \beta$ titanium alloys. Figure 15a shows the IPF map overlaid on the fatigue microspecimen and Figure 15b depicts the orientation of the prism (green) and basal (purple) planes for various grains within the gage section of this specimen. Comparing Figure 15 with Figure 13, it is clear that grain 1 exhibits evidence of basal slip activity, while the adjacent grain, labeled as grain 2, deforms via prism slip based on the orientation of the slip lines and the plane traces determined via EBSD. This is the first specimen tested to exhibit a noticeable accumulation of basal slip, which agrees with the work of Bridier in which basal slip is the critical slip mode for $\alpha + \beta$ titanium alloys under cyclic loading conditions, whereas predominantly prism slip was activated in tension.[10]

In comparing the crystallographic orientations of the $\alpha_p$ grains relative to the adjacent transformed $\beta$ material shown in Figure 15, it does not appear that the Burgers orientation relationship is maintained in these $\alpha_p$ grains. Thus, the Burgers orientation relationship is not a critical factor in the localization of fatigue damage in this specimen. This is supported by the fact that no slip lines appear in any of the adjacent $\alpha$ laths for this specimen. Although, this is simply based on a surface observation, so subsequent 3D serial sectioning of microspecimens will provide a more comprehensive description of fatigue critical microstructural neighborhoods.

**Discussion**

*Effect of Strain Rate in Microscale Tension Tests*

Although other researchers have observed the reduction in mechanical properties as a function of decreasing sample size,[29,30] the disparity in measured values of yield strength between bulk and microscale specimens may also be affected by the effective strain rate of the tensile tests. Conventional tests are typically conducted at strain rates of approximately $10^{-3}s^{-1}$. In microscale tension tests, the strain rate was set at $1.9 \times 10^{-3}s^{-1}$ to reasonably approximate conventional rates, while also proceeding slowly enough to allow for multiple images to be acquired to document localization of deformation before specimen fracture. However, the microscale tests are interrupted after every 0.1 μm of crosshead displacement to acquire an image. The high resolution images take approximately 3 minutes to acquire. Therefore, even though the displacement rates are similar, the effective strain rates of these two test techniques are much different, with the effective strain rate of microscale specimens being $1.25 \times 10^{-5}$. In conventional testing of Ti-6Al-4V, slower strain rates are known to produce lower yield strength and flow strength.[43] Zhou and Chew observed approximately a 9% decrease in the 0.2% yield stress for tests conducted at $4.68 \times 10^{-5}$ $s^{-1}$ compared with tests conducted at $4.68 \times 10^{-3}$ $s^{-1}$, which is nearly the same range of effective strain rates that were employed in the microscale tests. Strain rate is likely to influence microscale test results, and in fact the effect of strain rate may be enhanced in microscale tests due to the significant impact that individual grains may have in microscale tests relative to conventional laboratory samples. Therefore, it is clear that strain rate likely plays a part in affecting microscale mechanical test results, although it does not appear to account for the total debit in properties. Future work will investigate the response to strain rate to quantify its affect on mechanical properties.

*Comparison of Microscale Tension with Microscale Fatigue Tests*

The specimens tested in fatigue appeared to be much stronger than the specimens tested in tension. For example, although all the tension samples were observed to yield and fail well below the bulk yield strength of 1140 MPa, the fatigue samples appeared to be much stronger than this. The disparity in strength between microscale tension and fatigue tests was unanticipated, but there are a few potential explanations. The effective strain rate of tension tests due to image acquisition has already been cited to be much slower in microscale testing compared with the strain rates of bulk specimens. Additionally, the fatigue test control method

may contribute to the difference in results. Since the test is not truly conducted in either displacement or load control, there may differences in the mechanical properties measured via this technique. As Figure 6a illustrates, there is no obvious load relaxation occurring during the blocks of fatigue cycles following the quasi-static calibration procedure. Thus, it does not appear that the observed fatigue behavior is significantly affected by the test control method. However, given that these specimens are not tested under load control condition, which are dynamically controlled, there is a possibility that the testing protocol is affecting the results. Future work is planned to develop control software capable of running microscale fatigue tests via dynamic load control.

*Sources of Error*

There are some extrinsic factors that likely affect the mechanical properties measured in these specimens, including: accurate measurement of cross sectional area and alignment of the load train. The cross sectional area of these specimens is difficult to measure accurately due to their unique shape. Since these specimens are not cylindrical, their cross sectional area needs to be calculated based on geometric relationships. The assumptions inherent in using these geometric relationships introduce error, since these specimens do not have perfect edges and corners. The effect of this error has been mitigated by utilizing measurements from multiple perspectives.

Sample misalignment will yield artificially low mechanical properties due to bending, as documented by Kim and co-workers.[33] This error is lessened, although not eliminated via careful seating and alignment of the specimen within the grips to ensure that the specimen is centered and contacts both edges of the grip simultaneously. The viewing perspective in the microscope provides high resolution observation of misalignment in this plane. However, it is difficult to ensure that no bending moment is induced in the specimen about either of the axes in the plane of the screen. For this type of misalignment, we have attempted to mitigate bending via the specimen grip geometry. The grip is machined at the end of a long silicon fiber, which provides high lateral compliance. Thus, very little lateral restoring force is transmitted to the specimen in any of the non-axial directions.

## Conclusions

This paper has demonstrated the adaptation of a microscale tension testing technique to enable *in-situ* microscale fatigue testing. This technique has been demonstrated to be an effective method for observing microstructurally-sensitive localized damage accumulation. Additionally, this technique may be used to probe the strength of specific targeted microstructural regions, such as regions of microtexture. Furthermore, slip accumulation occurs preferentially at phase interfaces by either a mechanism of slip transmission across interfaces or via a mechanism of slip incompatibility at those interfaces. The activation of these various modes of damage accumulation has been shown to result from the orientation of the grains and microstructural features in these local neighborhoods. In both tension and fatigue tests, localized slip is first observed in the α phase constituent in either the $\alpha_p$ grains or secondary α laths.

Yield strengths in microscale specimens approximately 20 um in diameter do not match the results observed in conventional laboratory-scale specimens, nor do they exhibit stronger mechanical properties, as typically reported. This has been attributed to the fact that nearly all grains in the microspecimens are touching the specimen surface, and as a result they experience much less constraint compared with the grains in the interior of conventional laboratory scale fatigue specimens. Additionally, the monotonic microscale strengths reported here do not match single crystal scale microspecimens, as the presence of multiple interfaces and boundaries are believed to provide suitable dislocation sources. In addition to these factors, it is possible that a combination of testing parameters may affect the observed monotonic strength of these specimens. These factors include experimental error in measurement of specimen cross sectional area, specimen alignment, or the relatively low effective strain rates resulting from the extended time required for image acquisition. Under fatigue loading conditions, specimens appear to have better mechanical properties relative to conventional laboratory scale specimens. The reasons for this are not entirely clear at this point, but future investigations will focus on the effect of frequency and endeavor to cycle specimens for longer times to determine if strain will continue to accumulate as testing continues.

The slip systems that are activated in microscale tests replicate the active slip systems observed in conventional laboratory scale tension and fatigue tests. The observation of similar slip activity indicates that data from these specimens may be useful in the calibration of crystal plasticity and

fracture models. Future work will address the role of frequency and loading rate on the mechanical properties of specimens of this size. Additionally, microscale tests will be integrated with digital image correlation and 3D serial sectioning experiments to quantify strain and to relate this strain accumulation to specific microstructural locations where localized plasticity is observed.

**Acknowledgements**

Financial support from the AFOSR Structural Mechanics Program (Dr. David Stargel, Project # 2302DR1P) is gratefully acknowledged. Many useful technical discussions with Drs. Mike Uchic and Reji John increased the technical merit of this work. The authors gratefully acknowledge Mr. Adam Shiveley for his assistance with adapting the LabView control software to enable accurate and repeatable fatigue testing and Mr. Alan Smith in using the micro-EDM to facilitate the machining of microscale mechanical specimens.

**References**

[1] Jha SK, Larsen JM, Rosenberger AH, Hartman GA. Scripta Mater 2003; 48: 1637-42.

[2] Szczepanski CJ, Jha SK, Larsen JM, Jones, JW. Metall Mater Trans A 2008; 39A: 2841-51.

[3] Jha SK, Larsen JM. VHCF-4, In: Proceedings of the fourth international conference on very high cycle fatigue. 2007. p. 385–96.

[4] Jha SK, Szczepanski CJ, Golden PJ, Porter III WJ, John R, Int J Fat 2012; 42: 248-57.

[5] Luetjering G, Peters M. EPRI CS 2933. Project 1266-1. Final Report – Electric Power Research Institute, Palo Alto, California , October 1983.

[6] Bowen AW. Acta Metall., 1975; 23: 1401-9.

[7] Larson F, Zarkades A. MCIC Report - MCIC·74-20 – Metals and Ceramics Information Center, Columbus, OH, June 1974.

[8] Pilchak AL, Williams REA, Williams JC. Metall Mater Trans A 2010; 41A: 106–24.

[9] Bantounas I, Dye D, Lindley TC, Acta Materialia 2009; 57: 3584–95.

[10] - Bridier F, Villechaise P, Mendez J. Acta Materialia 2008; 56: 3951–62.

[11] Williams JC, Baggerly RG, Paton NE. Metall Mater Trans A 2002; 33A:837-50.

[12] Neal DF, Blenkinsop PA. Acta Metall 1976; 24: 59–63.

[13] Mahajan Y, Margolin H. Metall Trans A 1982; 13A: 257–68.

[14] Evans WJ, Mater Sci Eng A, 1998 A243:89–96.

[15] Bache, MR. Int J Fat 2003; 25: 1079–87.

[16] Pilchak AL, Williams, JC. Metall Mater Trans A, 2011; 42: 1000-27.

[17] Le Biavant K, Pommier S, Prioul C. Fat Fract Eng Mater Struct 2002; 25: 527–45.

[18] Mills MJ, Hou DH, Suri S, Viswanathan GB. In: Boundaries and Interfaces in Materials, 1998, TMS, Warrendale, PA, p. 295.

[19] Savage MF, Tatalovich J, Zupan M, Hemker KJ, Mills MJ. Mater Sci Eng A 2001; 319-321: 398–403.

[20] Suri S, Viswanathan GB, Neeraj T, Hou D, Mills MJ. Acta Mater 1999; 47: 1019–34.

[21] Gianola DS, Sedlmayr A, Monig R, Volkert CA, Major RC, Cyrankowski E, Asif SAS, Warren OL, Kraft O, Rev Sci Inst 2011; 82, 063901.

[22] Greer JA, De Hosson JTM, Prog Mater Sci 2011; 56: 654–724.

[23] Uchic MD, Shade PA, Dimiduk DM. Ann Rev Mater Res 2009; 39: 361–86.

[24] Kraft O, Gruber PA, Monig R, Weygand D. Ann Rev Mater Res 2010; 40: 293–317.

[25] Uchic MD, Dimiduk DM, Florando JN, Nix WD, Science 2004; 305, 986-9, DOI: 10.1126/science.1098993.
[26] Uchic MD, Dimiduk DM, Wheeler R, Shade PA, Fraser HL. Scripta Mater 2006; 54: 759-64.
[27] Shade PA, Uchic MD, Dimiduk DM, Viswanathan GB, Wheeler R, Fraser HL. Mater Sci Eng A 2012; 535: 53-61.
[28] Norfleet DM. The Ohio State University, Ph.D. Thesis. 2007.
[29] Yang B, Motz C, Grosinger W, Dehm G, Fatigue 2010, Procedia Eng 2010; 2: 925–30.
[30] Janssen PJM, de Keijser TH, Geers MGD. Mater Sci Eng A 2006; 419: 238-48.
[31] Miyazaki S, Shibata K, Fujita H. Acta Metall 1979; 27: 855-62.
[32] Khatibi G, Betzwar-Kotas A, Groger V, Weiss B. Fat Fract Eng Mat Struct 2005; 28: 723-33. doi: 10.1111/j.1460-2695.2005.00898.x
[33] Kim S-W, Oh C-S, Lee H-J. Fat Fract Eng Mater Struct 2006; 30: 64–71. doi: 10.1111/j.1460-2695.2006.01089.x
[34] Yang B, Motz C, Grosinger W, Dehm G. Mater Sci Eng A 2009; 515: 71–8.
[35] Lu H, Shi HG, Zhou M. Fatigue Fract Eng Mater Struct 30, 87–94, doi: 10.1111/j.1460-2695.2006.01078.x
[36] Eberl C, Riesch-Oppermann H, Spolenak R, Kubat F, Ruile W, Courty D, Kraft O. IEEE Trans Dev Mat Reliability 2010; 10: 366-73.
[37] Eberl C, Spolenak R, Arzt E, Kubat F, Leidl A, Ruile W, Kraft O. Mater Sci Eng A 2006; 421: 68–76.
[38] Muhlstein CL, Stach EA, Ritchie RO. Acta Mater 2002; 50: 3579–95.
[39] Uchic MD, Dimiduk DM. Mater Sci Eng A 2005; 400–401: 268–78.
[40] Shade PA, Wheeler R, Choi YS, Uchic MD, Dimiduk DM, Fraser HL. Acta Mater 2009; 57: 4580–7.
[41] Wheeler R, Shade PA, Uchic MD. J Mater (JOM) 2012; 64: 58-65.
[42] Bridier F, Villechaise P, Mendez J. Acta Mater 2005; 53: 555–67.
[43] Zhou W, Chew KG. J Mater Sci 2002; 37: 5159–65.

**Figure Captions**

Figure 1. Backscattered electron (BSE) micrograph of the duplex microstructural condition investigated in this study. The dark equiaxed features are $\alpha_p$ grains, the matrix phase is transformed β, which is composed of lath α and retained β.

Figure 2. Inverse pole figure maps (IPFs) of (a) the α phase constituent, (b) the α phase particles with an orientation favorable for easy basal slip (Schmid Factor ≥ 0.475), and (c) the α phase particles with an orientation suitable for easy prism slip (Schmid Factor ≥ 0.475).

Figure 3. Secondary electron (SE) micrograph of microscale specimens viewed at 45° angle in various stages of completion. The left two pillars are shown after micro-EDM machining and the three specimens on the right have had subsequent FIB machining.

Figure 4. A secondary electron (SE) micrograph of a typical microscale specimen, with a typical gage length of approximately 50 μm and grip diameter of 40 μm.

Figure 5. A schematic of the microtesting fixture used to perform the *in-situ* tests in this study. Adapted from [40].

Figure 6. Load traces acquired from the data acquisition system. (a) Load trace for one hour exhibits four full blocks of fatigue loading cycles, the intermediate image acquisition times and the calibration procedures employed during a fatigue test. (b) Load trace for a ten second period of time illustrating a repeatable sinusoidal loading profile.

Figure 7. The stress-strain curve for the microscale specimens shown relative to conventional laboratory scale specimens.

Figure 8. Microscale specimen deformed in tension shown: (a) prior to testing with α phase IPF map overlay, (b) prior to testing overlaid with plane traces basal (purple) and prism (green) planes, and (c) in the image preceding failure where slip lines are observed to be continuous across the lath and an adjacent $\alpha_p$ grain.

Figure 9. Microscale specimen deformed in tension shown: (a) prior to testing with $\alpha$ phase IPF map overlay, (b) prior to testing overlaid with plane traces basal (purple) and prism (green) planes, and (c) in the image preceding failure where slip is observed to accumulate at lath interfaces and at phase boundaries without any evidence of transmission across phase boundaries.

Figure 10. Microscale specimen shown in Figure 9 shown overlaid with Schmid Factor maps calculated based on the macroscopically applied load for: (a) prism and (b) basal slip.

Figure 11. S-N plot illustrating the superior fatigue behavior of microscale specimens relative to the conventional fatigue specimens. Adapted from [2].

Figure 12. (a) Microscale fatigue specimen with exploded views of the region where localized plasticity is observed to accumulate after testing at (b) $\sigma_{max}$ = 860 cycles for $10^7$ cycles, (c) $\sigma_{max}$ = 920 cycles for $10^7$ cycles, and (d) $\sigma_{max}$ = 980 cycles for $10^7$ cycles.

Figure 13. (a) Microscale specimen tested in fatigue with exploded views of the grains 1 and 2 where localized plasticity is observed to accumulate after (b) N=0 cycles, (c) N=43,000 cycles, and (d) N=100,000 cycles.

Figure 14. Plot of total measured strain as a function of testing time indicating that strain continues to accumulate as fatigue cycling continues.

Figure 15. (a) IPF map overlaid on the microscale fatigue specimen shown in Figure 13. (b) Plane traces for basal (purple) and prism (green) planes overlaid on a micrograph of the fatigue specimen. Grains 1 and 2 labeled in this figure correspond to the labels in Figure 13.

**Figures**

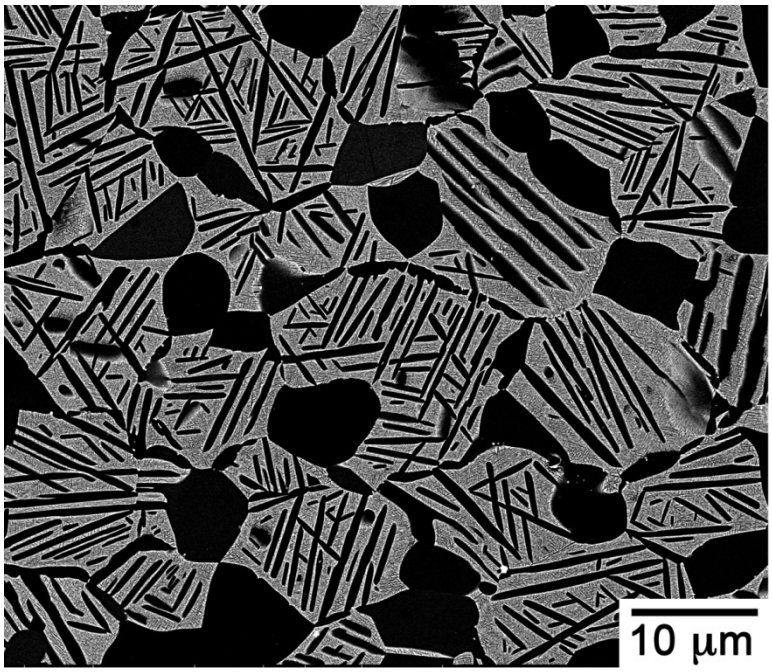


Figure 1.

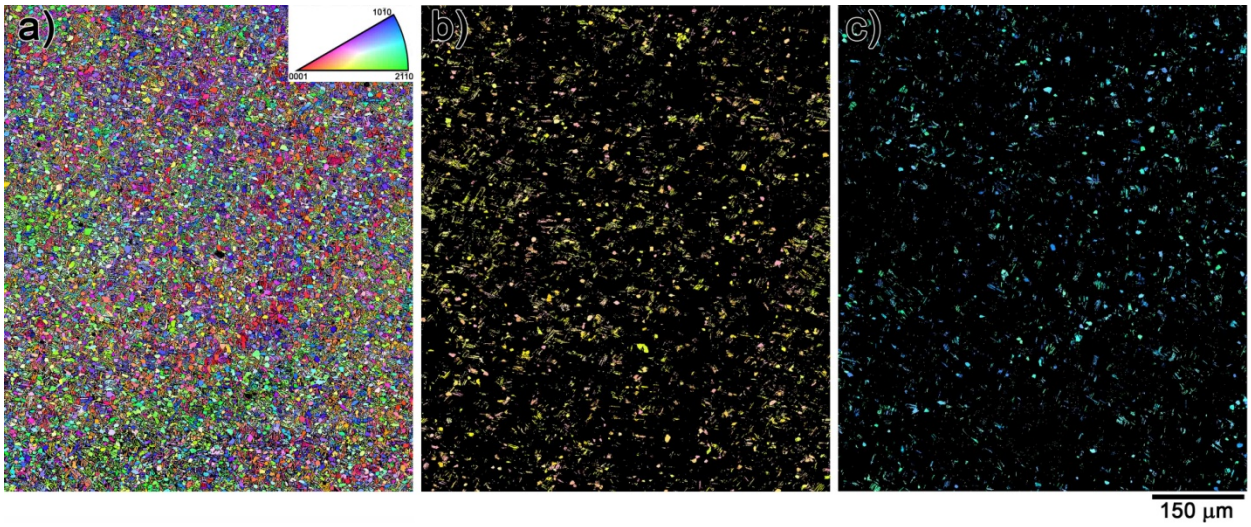


Figure 2.

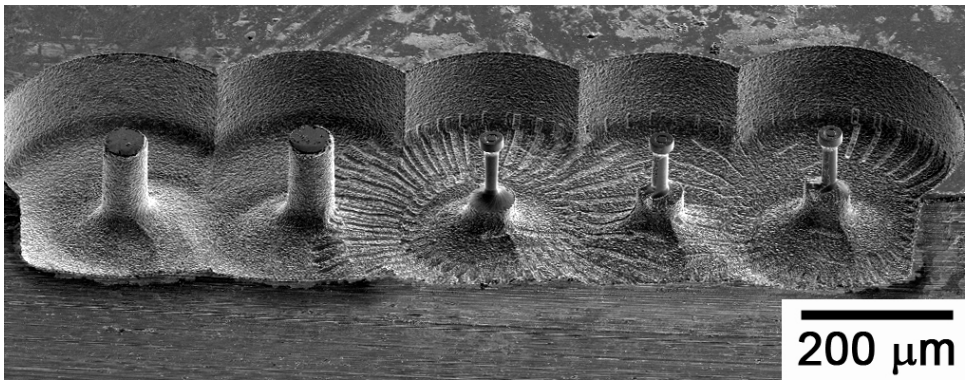


Figure 3.

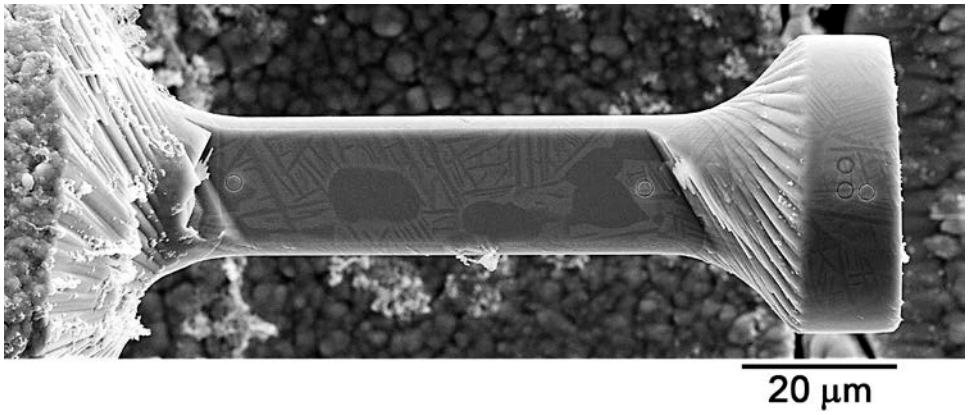


Figure 4.

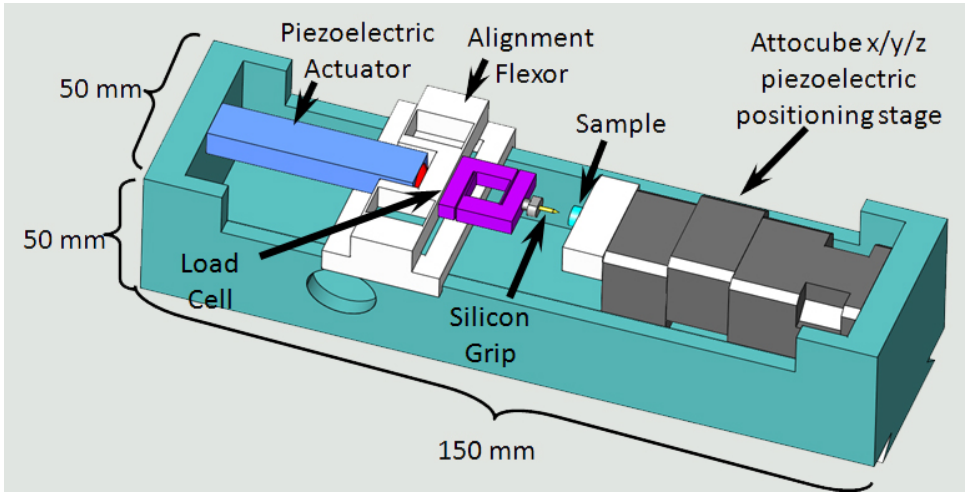


Figure 5.

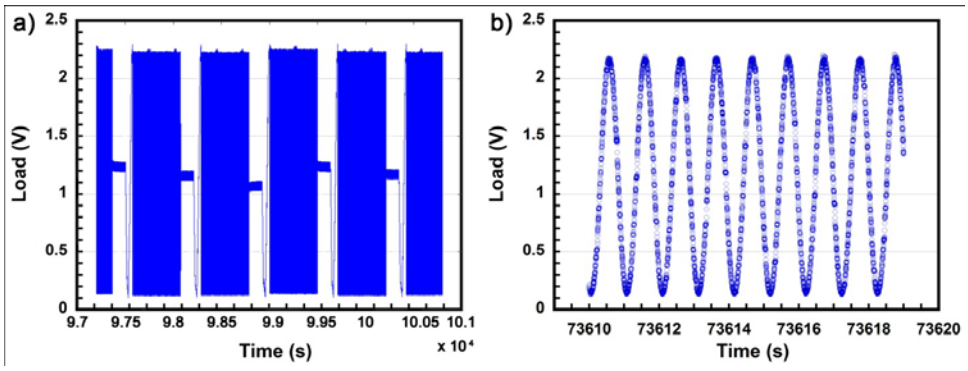


Figure 6.

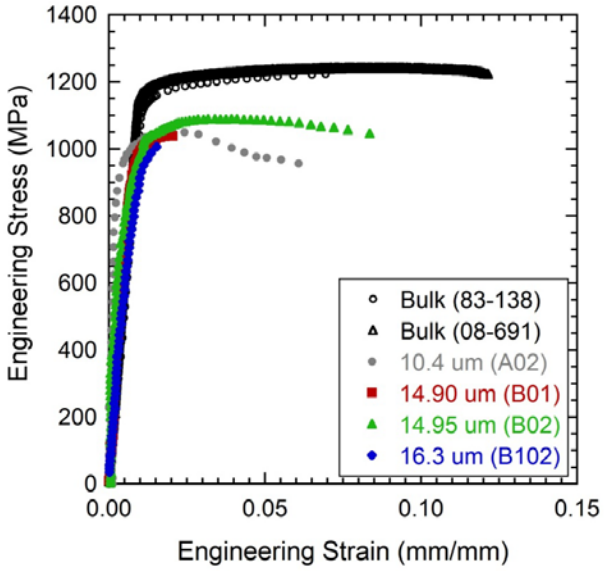


Figure 7.

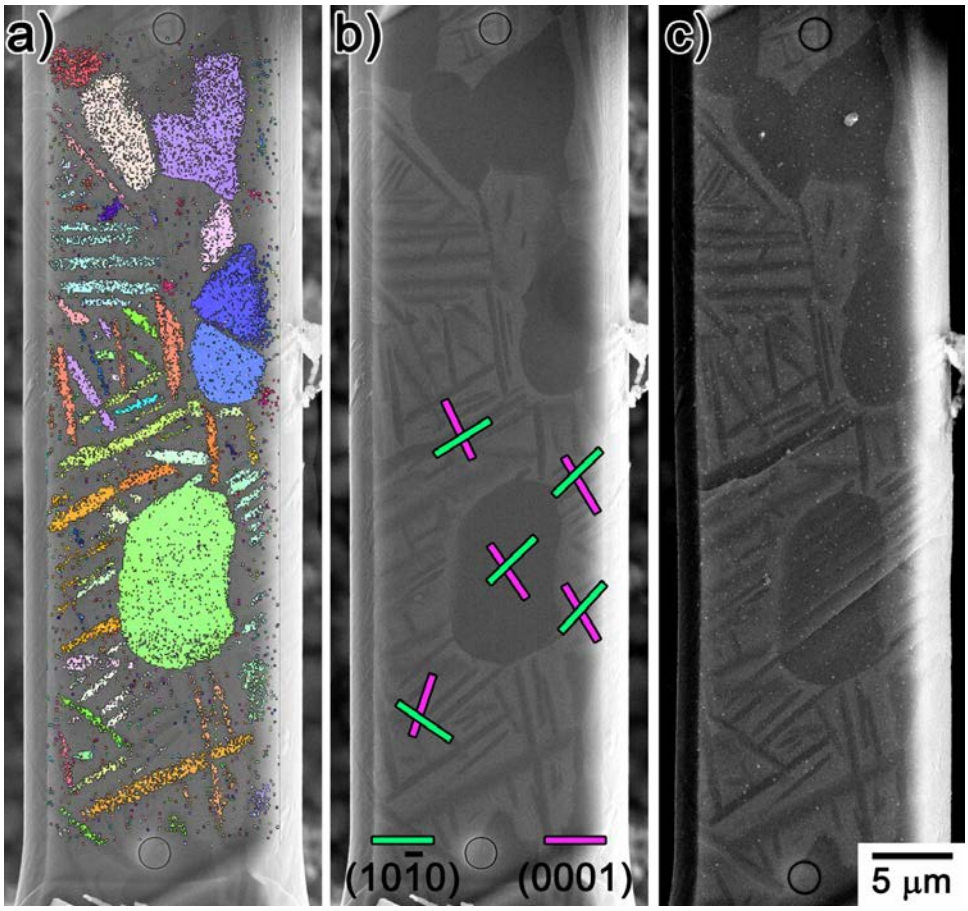


Figure 8.

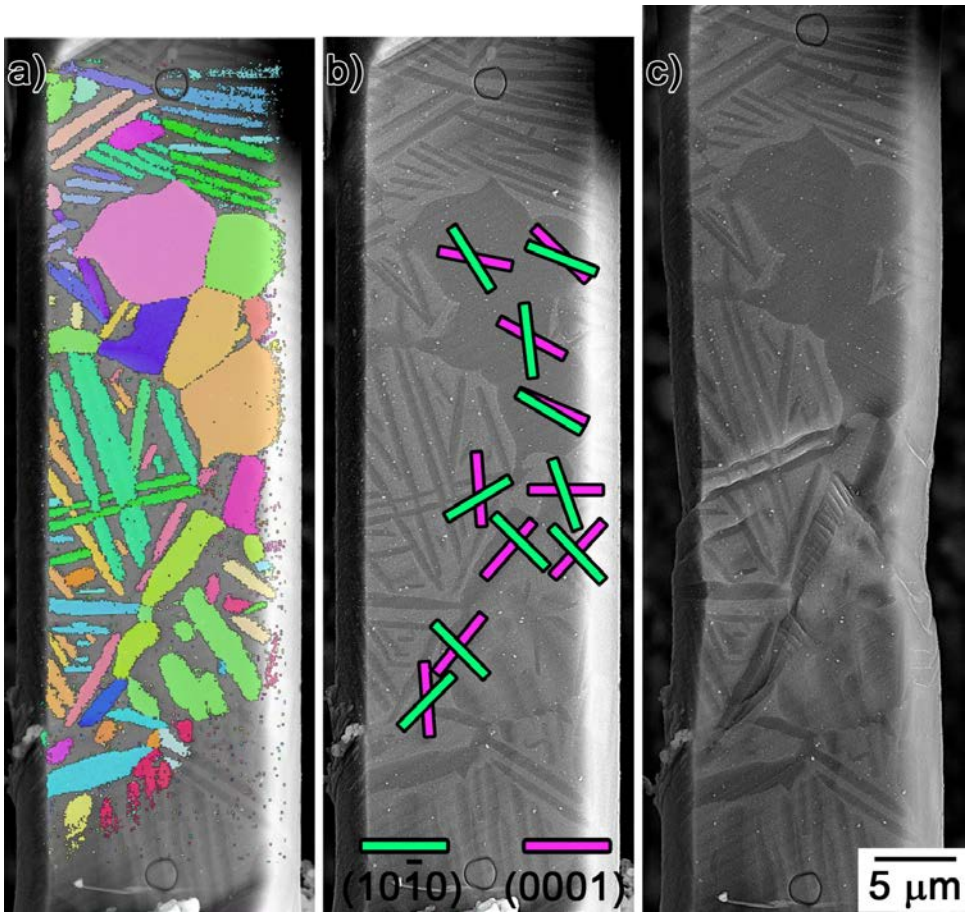


Figure 9.

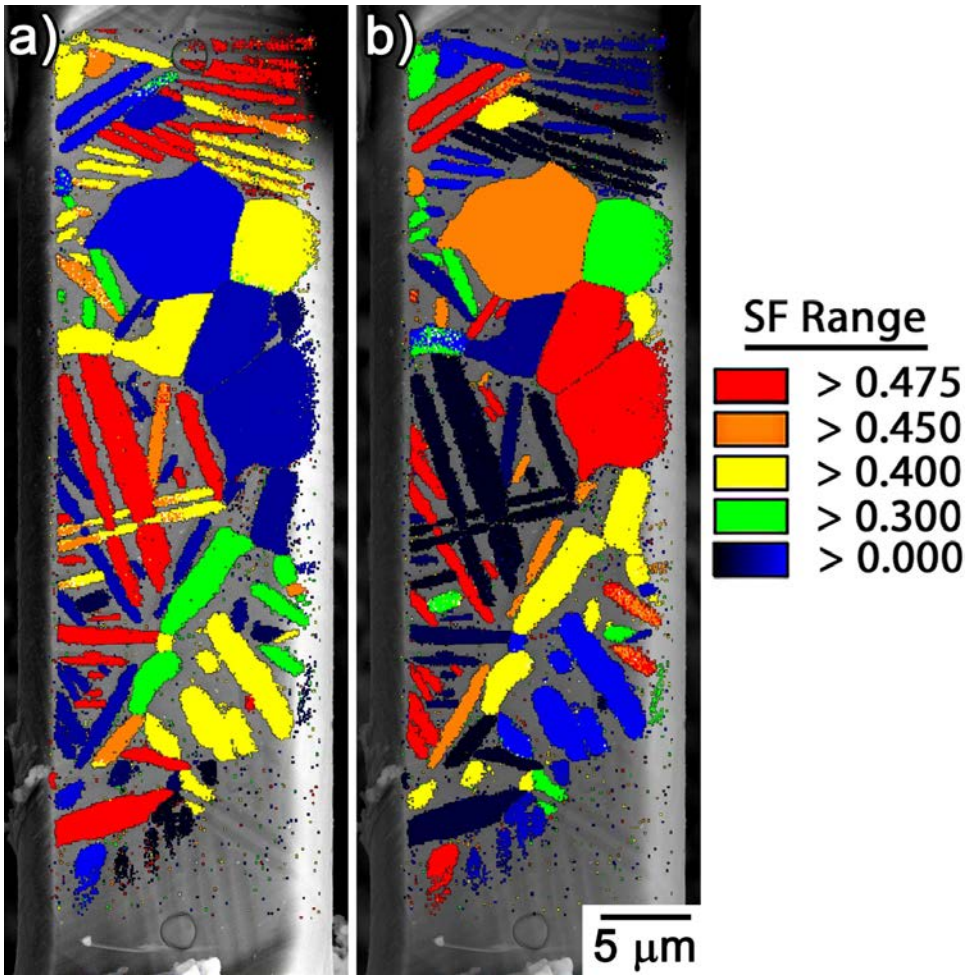


Figure 10.

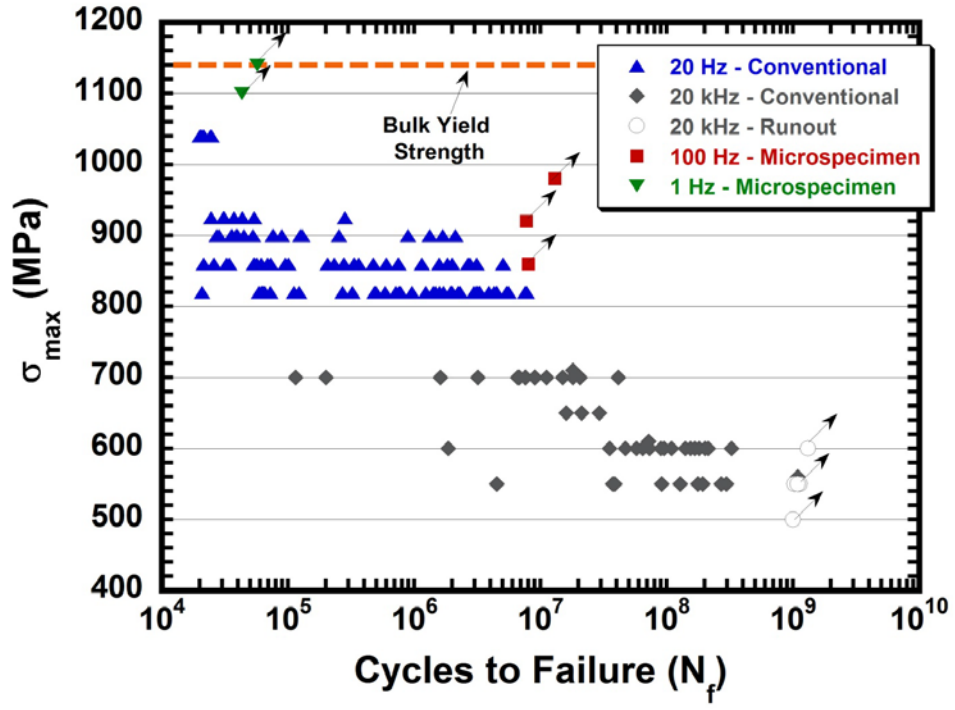


Figure 11.

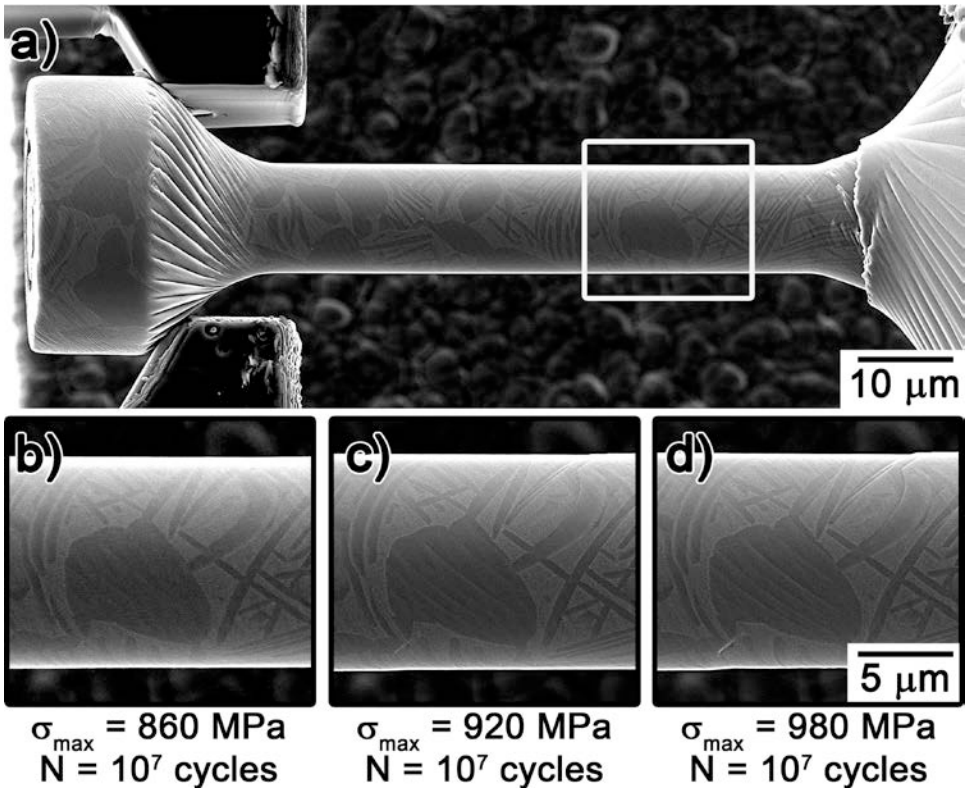


Figure 12

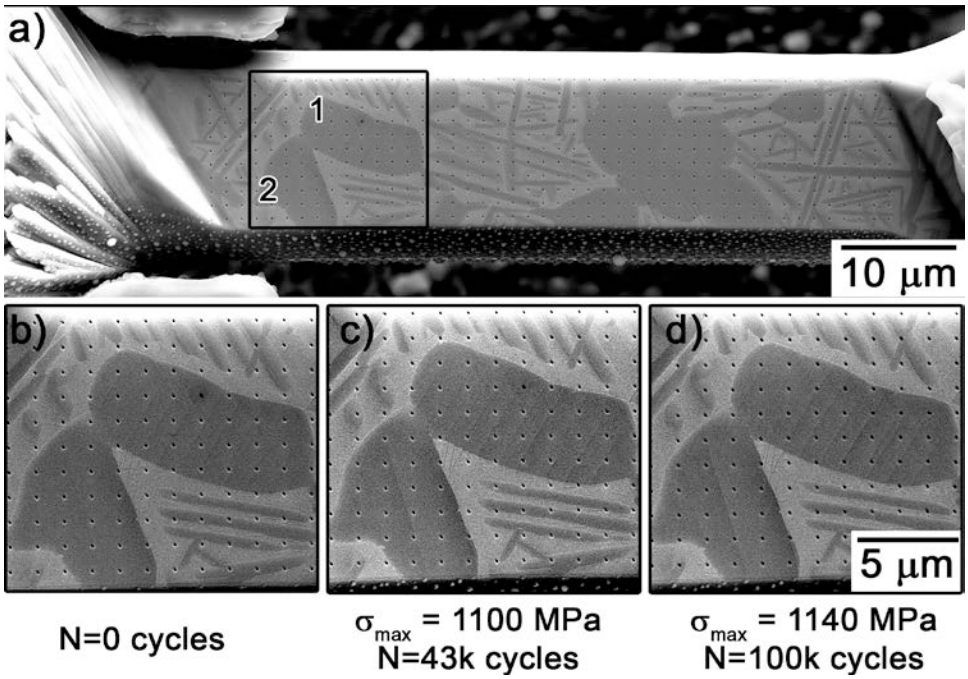


Figure 13.

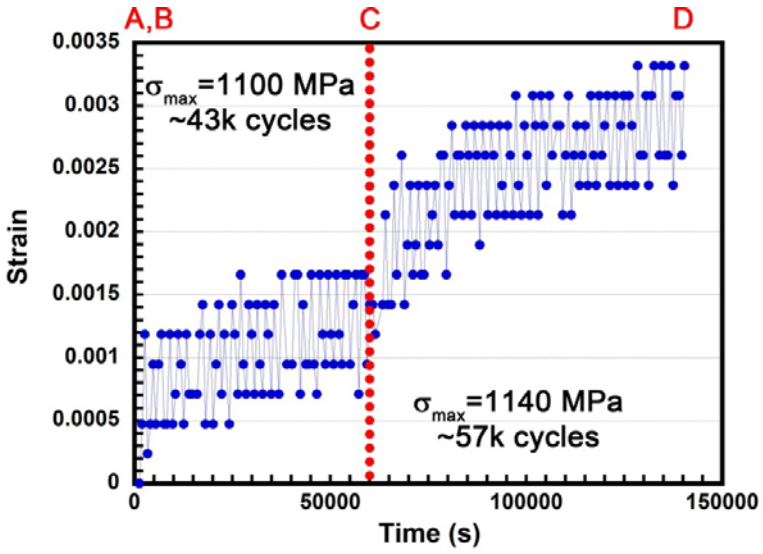


Figure 14

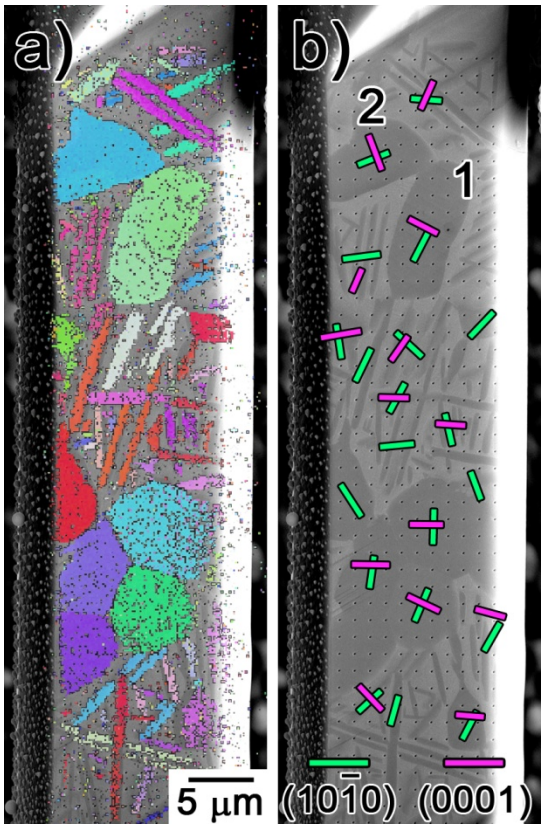


Figure 15.